International Journal of Pharmaceutics: X 5 (2023) 100169

Contents lists available at ScienceDirect

International Journal of Pharmaceutics: X

journal homepage: www.sciencedirect.com/journal/international-journal-of-pharmaceutics-x

Antibiotic-loaded hydroxyapatite scaffolds fabricated from *Nile tilapia* bones for orthopaedics

Atchara Khamkongkaeo [a], Arreerat Jiamprasertboon [b,c], Nanthawan Jinakul [d], Phatraya Srabua [e], Saran Tantavisut [f,g], Amaraporn Wongrakpanich [h,*]

[a] *Department of Metallurgical Engineering, Faculty of Engineering, Chulalongkorn University, Bangkok, Thailand*
[b] *School of Chemistry, Institute of Science, Suranaree University of Technology, Nakhon Ratchasima, Thailand*
[c] *Institute of Research and Development, Suranaree University of Technology, Nakhon Ratchasima, Thailand*
[d] *Department of Microbiology, Faculty of Pharmacy, Mahidol University, Bangkok, Thailand*
[e] *Scientific and Technological Research Equipment Center (STREC), Chulalongkorn University, Bangkok, Thailand*
[f] *Department of Orthopaedics, Chulalongkorn University, Bangkok, Thailand*
[g] *Hip Fracture Research Unit, Department of Orthopaedics, Chulalongkorn University, Bangkok, Thailand*
[h] *Department of Pharmacy, Faculty of Pharmacy, Mahidol University, Bangkok, Thailand*

ARTICLE INFO

Keywords:
Hydroxyapatite
Scaffold
Vancomycin
Antibiotic
Antibiotic-coated
Antibiotic-loaded
Nile tilapia

ABSTRACT

This work aimed to develop new antibiotic-coated/ antibiotic-loaded hydroxyapatite (HAp) scaffolds for orthopaedic trauma, specifically to treat the infection after fixation of skeletal fracture. The HAp scaffolds were fabricated from the Nile tilapia (*Oreochromis niloticus)* bones and fully characterized. The HAp scaffolds were coated with 12 formulations of poly (lactic-*co*-glycolic acid) (PLGA) or poly (lactic acid) (PLA), blended with vancomycin. The vancomycin release, surface morphology, antibacterial properties, and the cytocompatibility of the scaffolds were conducted.

The HAp powder contains elements identical to those found in human bones. This HAp powder is suitable as a starting material to build scaffolds. After the scaffold fabrication, The ratio of HAp to β-TCP changed, and the phase transformation of β-TCP to α-TCP was observed. All antibiotic-coated/ antibiotic-loaded HAp scaffolds can release vancomycin into the phosphate-buffered saline (PBS) solution. PLGA-coated scaffolds obtained faster drug release profiles than PLA-coated scaffolds. The low polymer concentration in the coating solutions (20%*w/v*) gave a faster drug release profile than the high polymer concentration (40%w/v). All groups showed a trace of surface erosion after being submerged in PBS for 14 days. Most of the extracts can inhibit *Staphylococcus aureus* (*S. aureus)* and methicillin-resistant *S. aureus* (MRSA). The extracts not only caused no cytotoxicity to Saos-2 bone cells but also can increase cell growth. This study demonstrates that it is possible to use these antibiotic-coated/ antibiotic-loaded scaffolds in the clinic as an antibiotic bead replacement.

Abbreviations: α-TCP, α-tricalcium phosphate; β-TCP, β-tricalcium phosphate; CLSI, The Clinical and Laboratory Standards Institute; DI, Deionized water; DMSO, Dimethyl sulfoxide; F1[V-PLGA20-Lvanc], Formulation 1, HAp saffolds containing low concentration of *v*ancomycin, coated with PLGA 20%*w/v* blended with vancomycin; F2[V-PLGA40-Lvanc], Formulation 2, HAp saffolds containing low concentration of vancomycin, coated with PLGA 40%*w/v* blended with vancomycin; F3[V-PLA20-Lvanc], Formulation 3, HAp saffolds containing low concentration of vancomycin, coated with PLA 20%*w/v* blended with vancomycin; F4[V-PLA40-Lvanc], Formulation 4, HAp saffolds containing low concentration of vancomycin, coated with PLA 40%*w/v* blended with vancomycin; F5[PLGA20-Lvanc], Formulation 5, HAp saffolds containing low concentration of *v*ancomycin, coated with PLGA 20%*w/v*; F6[PLGA40-Lvanc], Formulation 6, HAp saffolds containing low concentration of *v*ancomycin, coated with PLGA 40%*w/v*; F7[PLA20-Lvanc], Formulation 7, HAp saffolds containing low concentration of vancomycin, coated with PLA 20%*w/v*; F8[PLA40-Lvanc], Formulation 8, HAp saffolds containing low concentration of vancomycin, coated with PLA 40%*w/v*; F9[PLGA20-Hvanc], Formulation 9, HAp saffolds containing high concentration of vancomycin, coated with PLGA 20%*w/v*; F10[PLGA40-Hvanc], Formulation 10, HAp saffolds containing high concentration of vancomycin, coated with PLGA 40%*w/v*; F11[PLA20-Hvanc], Formulation 11, HAp saffolds containing high concentration of vancomycin, coated with PLA 20%*w/v*; F12[PLA40-Hvanc], Formulation 12, HAp saffolds containing high concentration of vancomycin, coated with PLA 40%w/v; FDA, Food and Drug Administration; FTIR, Fourier transforms infrared spectroscopy; HAp, Hydroxyapatite; IFSF, The infection after fixation of skeletal fracture; P.U., Polyurethane; PBS, Phosphate-buffered saline; PLA, Poly(lactic acid); PLGA, Poly(lactic-co-glycolic acid); PVA, Polyvinyl alcohol; SEM, Scanning electron microscopy; XRD, X-ray diffraction; XRF, X-ray fluorescence spectroscopy.

* Corresponding author.
E-mail address: amaraporn.won@mahidol.ac.th (A. Wongrakpanich).

https://doi.org/10.1016/j.ijpx.2023.100169
Received 26 October 2022; Received in revised form 1 February 2023; Accepted 5 February 2023
Available online 8 February 2023

1. Introduction

Infection is one of the most serious complications after operative fixation of the skeletal fracture. The infection after fixation of skeletal fracture (IFSF) incidence ranges from 1% to 30%, depending on the severity of bone damage, soft-tissue trauma, and contamination level (Morgenstern et al., 2018; Baertl et al., 2021). The IFSF can compromise fracture healing, severely affect clinical outcomes, and increase morbidity and mortality rates. IFSF can be treated using various methods, i.e., systemic antibiotic(s), adequate debridement and irrigation, implant retention/removal decision, and local antimicrobial therapy (Foster et al., 2020a; Depypere et al., 2020). Local antibiotic administration has attracted considerable interest in IFSF treatment. Generally, antibiotics such as vancomycin, gentamicin, and tobramycin, alone or in combination (Qiu et al., 2018; Tantavisut et al., 2022), have been mixed with bone cement to create a local drug delivery system in the form of polymethylmethacrylate beads (Qiu et al., 2017; Shinsako et al., 2008; Taggart et al., 2002; van Vugt et al., 2019). In most cases, these beads can cure the infection and prevent biofilm formation. However, they must be removed during the second operation or when the wound is closed (Foster et al., 2020b). In addition, after prolonged antibiotic elution, the level of antibiotic concentration at the bone cement surface might be low and prone to become an additional attachment surface to bacteria, potentially leading to ongoing infection and creating antibiotic-resistant bacteria (Neut et al., 2001; Schmolders et al., 2014). Using a fully biodegradable implant is an attractive alternative to traditional beads. The new biodegradable implant can deliver a high concentration of antibiotic(s) to the infection site and does not require removal.

Bioresorbable materials such as calcium sulfate and hydroxyapatite are being studied extensively to solve known problems with antibiotic (s)-loaded bone cement. When compared to bone cement, these materials can eliminate foreign body problems, do not require removal procedures, can be used with a broader range of antibiotics, and promote bone healing, making them ideal for IFSF situations.

Hydroxyapatite (HAp) is a well-known calcium phosphate biomaterial with the chemical composition $Ca_{10}(PO_4)_6(OH)_2$, identical to the mineral phase of bone and the hard tissues of humans. HAp can enhance osteoblast attachment and viability (O'Hare et al., 2010). It can interact with living bone tissue without causing cytotoxicity or inflammatory response. These desired properties made HAp a good candidate for biomedical applications, especially in orthopaedic (Petit, 1999). To date, there are various forms of HAp, such as the coating on porous metals, fine granules, powders, and composites (Oonishi, 1991; Meirelles et al., 2008; Feng et al., 2022). HAp can be synthesized chemically or extracted from natural sources. Different sources and extraction methods would give different calcium-to-phosphate ratios, crystalline phases, and particle sizes/shapes. Most natural sources of HAp come from mammalian bones, i.e., bovine, camel, horse, and porcine (Mohd Pu'ad et al., 2019). Until recently, HAp from fish bone has emerged as an alternative source that is abundant, inexpensive, and safe, with minimal risks of disease transmission (Granito et al., 2018; Marliana et al., 2015; Shi et al., 2018). Since HAp extraction from fish bone is relatively new, most studies focused on the extraction methods and the material characterization (Firdaus Hussin et al., 2022). There are several knowledge gaps regarding the drug/polymer coating and the biomedical application of HAp from the fishbone.

Poly (lactic-*co*-glycolic) acid (PLGA) and poly (lactic acid) (PLA) are the most promising polymers for biomedical applications. They are Food and Drug Administration (FDA)-approved biodegradable polymers with biocompatible properties. They offer safe and non-toxic degradation products, making them suitable for various pharmaceutical applications. PLGA has been extensively studied as a drug delivery system that can entrap a wide range of actives, from small molecules to proteins (Makadia and Siegel, 2011a). PLGA is commonly used in orthopaedic applications (Zhao et al., 2021). PLGA in micro- and nanoparticle forms can act as a delivery system for growth factors in bone tissue engineering, such as the bone morphogenetic protein 2 (BMP2) (Ortega-Oller et al., 2015; Patel et al., 2021), vascular endothelial growth factor (*VEGF*) (Zhu et al., 2022), and transforming growth factor (TGF)-β3 (Park et al., 2016; Bouffi et al., 2010). Agarwal et al. (Agarwal et al., 2016) fabricated PLGA-silane coating on the magnesium alloy AZ31. This coating can improve cytocompatibility in MC3T3-E1 osteoblast cells (Agarwal et al., 2016). Because of its slow degradation profile, PLA has been used in clinical applications, mainly for medical devices and implants (Narayanan et al., 2016). PLA/magnesium composite show cytocompatibility with MC3T3-E1 osteoblast cells (Zhao et al., 2017). PLA can even be blended with HAp (Shuai et al., 2021), β-tricalcium phosphate (β-TCP) (Feng et al., 2018), and other materials (Shuai et al., 2022) to create a scaffold that contains bioactivity and osteoconductivity (Bernardo et al., 2022). Both polymers are compatible with bone cells and can potentially be used in orthopaedics for coating scaffolds/implants.

Taking all of these aspects into account, it is feasible to fabricate a HAp scaffold containing antibiotic(s) that inhibit bacterial growth without damaging the surrounding tissue and have a favorable effect on bone cells when released at the infected site. Furthermore, this scaffold should be fully biodegradable, avoiding the need for a second operation. This scaffold could be used to replace antibiotic beads. In this study, for the first time, the HAp scaffolds were fabricated using Nile tilapia (*Oreochromis niloticus*) bones. The HAp scaffolds were coated with PLGA or PLA blended with an antibiotic. Vancomycin was chosen as a drug model. The nanostructure of HAp was fully characterized in both powder and scaffold forms. The vancomycin release, surface morphology, antibacterial properties, and cytocompatibility of the antibiotic-coated/antibiotic-loaded HAp scaffolds were investigated.

2. Material and methods

2.1. Hydroxyapatite powder preparation

The hydroxyapatite powder (HAp) was extracted from the fish bone using the thermal decomposition method according to Khamkongkaeo et al. (Khamkongkaeo et al., 2021) with a modification in calcination temperature. The starting material was the Nile tilapia (*Oreochromis niloticus*) bones. The bones were collected, boiled to remove the organic impurities, dried, and cut into small pieces. The dried fish bone was calcined at 700 °C in an electrical furnace (Xinkyo, SX2–4-17TP, China) with a heating rate of 5 °C/min for 3 h. Before scaffold fabrication, the HAp powder was wet ball milled in deionized water (DI) using zirconia balls for 24 h to decrease particle size. Then a mixture was dried at 150 °C for 48 h to obtain the HAp powder for scaffold fabrication. The elemental composition of HAp powder was identified using the X-ray fluorescence spectroscopy, XRF (S8 Tiger, Bruker, USA), by measuring a characteristic X-ray that emitted from a sample after a primary X-ray source excitation.

2.2. Scaffold preparation

The scaffolds were fabricated using the polyurethane (P.U.) sponge replication technique. Before the coating process, cylindrical P.U. sponges (30 ppi, 7.5 (dia) x 13 mm (h)) were treated with 1 M NaOH solution for 24 h to enhance the adhesion between the slurry and the P. U. sponge surface, followed by washing with DI water for three times and dried at 100 °C for 1 h. HAp slurry was prepared by mixing the 4 g of HAp powder with 10 mL of 5%*w/v* polyvinyl alcohol (PVA, BF17W, Ajax Finechem Pty LTD, New Zealand), then stirred at 200 rpm for 2 h at room temperature until a homogenous slurry was achieved. When the homogeneous slurry was reached, it was coated on the P.U. sponges three times, and the excess slurry was removed using the centrifugation method with compressed air. After that, the coated sponges were dried at 100 °C for 1 h. Finally, the obtained sponges were sintered in an

electric furnace (XINKYO, SX2–4-17TP, China) under air atmosphere following a heating program: (i) from room temperature to 600 °C with the heating rate of 1 °C/min for 1 h to remove P.U. sponge, (ii) the heating was continued with the rate of 5 °C/min up to 1400 °C with a duration time of 5 h for consolidation, and (iii) the sintered scaffolds were naturally cooled in the furnace.

2.3. Scaffold characterization

The functional groups in the range of 4000–500 cm^{-1} present in the HAp powder and scaffolds were investigated using Fourier transform infrared spectroscopy (FT-IR, Bruker TENSOR 27 FT-IR Spectrometer, Bruker Corporation, USA). Moreover, high-quality X-ray diffraction patterns (XRD, EMPYREAN, Malvern Panalytical, Netherlands) were collected in the 2θ of 10–90° with a step size of 0.02° and a scan time of 2 s per step. Rietveld refinement was achieved on the high-quality XRD patterns using TOPAS software. F.P. peak type, which is based on Lorentzian-type crystallite size and Gaussian-type strain, was adopted as a peak profile for fitting.

2.4. Fabrication of the antibiotic-coated/antibiotic-loaded scaffolds

In this work, two types of polymers which are poly (lactic-*co*-glycolic acid) (PLGA, 50:50, Lactel® absorbable polymer, Durect Corporation, USA, Lot no. 1143-19-01, 0.65 dL/g in HFIP) and poly (lactic acid) (PLA, Lactel®, Absorbable polymer, Durect Corporation, USA, Lot no. 1143-05-01, 1.16 dL/g in $CHCl_3$) was used. Vancomycin in the form of vancomycin hydrochloride was introduced into the system as an antibiotic prototype. Vancomycin hydrochloride (Lot no. 0000052170, A4230021) was kindly gifted from Siam Bheasach Co., Ltd., Thailand.

Three sets (12 formulations) of the antibiotic coating were prepared using different polymers, different amounts of polymer, and different amounts of *v*ancomycin per one scaffold. The first set (Formulation 1–4) was composed of PLGA and PLA at 20%*w/v* and 40%w/v with vancomycin dissolved in the coating solution. Moreover, the scaffolds were pretreated with a low dose of vancomycin. The second set (Formulation 5–8) was similar to the first set, except it contained no vancomycin in the coating solution. The last set (Formulation 9–12) was similar to the second set, except with a high dose of vancomycin in the scaffold. All formulation compositions are shown in Table 1.

To prepare the coating solution, PLGA or PLA was dissolved in dichloromethane (ACS grade, Burdick & Jackson, SK Chemicals, Korea) at the concentration of 20%*w/v* and 40%w/v. Vancomycin was dissolved in methanol (ACS grade, Honeywell, Burdick & Jackson, USA) with a concentration of 0.3%w/v. The drug-polymer solution was prepared by mixing PLGA or PLA solution with the vancomycin in a methanol solution. Before coating, all scaffolds were weight. Some were pretreated by adding the vancomycin (in ethanol solution) and dried. Afterward, the scaffold was dipped into the drug-polymer solution, dried at room temperature overnight, weighed, and kept in the desiccator until used.

2.5. Drug elution assay

The drug elusion assays or the release studies of vancomycin from the scaffolds were conducted in phosphate-buffered saline (1xPBS, ultrapure grade, 0.1 μm sterile filtered, Apsalagen, Thailand). The scaffolds have a disc-like shape with lightweight; some of them may float after coating. Thus, all antibiotic-coated/antibiotic-loaded scaffolds were put into a custom-made dissolution sinker (Supplementary fig. 1) before being placed in centrifuge tubes containing 30 mL of PBS. The samples were incubated in an incubator shaker (Mini Shaking Incubator, ES-60, Hangzhou Miu Instruments Co., Ltd., China) at 37 °C, 100 rpm. The samples (1000 μL of PBS-containing antibiotic) were removed and replaced with pre-warmed PBS at designated times (1, 4, 8, 24 h, 2, 3, 8, and 14 days). All samples were kept at −20 °C for further analysis. The PBS-containing antibiotic solutions were analyzed for vancomycin content and antimicrobial property. At the end of 14 days, the scaffolds were removed and rinsed well with sterile water for irritation (SWI, General Hospital Products Public Co., Ltd., Thailand) before being dried at 45 °C overnight (Memmert GmbH, Germany). The scaffolds were weighted and evaluated for surface morphology using SEM.

Vancomycin content in the PBS-containing antibiotic solutions was quantified using the spectrophotometric method. The drug moiety was quantified based on a coupling reaction between vancomycin and diazotized procaine with a validated protocol in a 96-well plate (Hadi, 2014). In short, the PBS-containing antibiotic solutions were mixed with procaine solution and 0.125 M ammonium hydroxide (NH_4OH, Carlo ERBA Reagents, USA) at a volume ratio of 100:30:120. Procaine solution is a mixture of 1.0 mM procaine hydrochloride (Sigma Life Science, USA), 1.0 M hydrochloric acid (HCl, Chem-Lab, Belgium), and 1.0 mM sodium nitrite ($NaNO_2$, Carlo ERBA Reagents, USA). The absorbance of the yellow color azo dye was measured at 447 nm using a microplate reader (ClarioStar Multimode Microplate Reader, BMG Labtech, Germany). Blank was prepared in the same way as the samples but used PBS instead of the PBS-containing antibiotic solutions. The vancomycin cumulative release profiles (μg, Y-axis) were plotted against time (hours, X-axis).

Table 1
Three sets (12 formulations) of the antibiotic coating and scaffold-pretreated solutions.

Formu-lation number	Formulation codename*	The drug-polymer coating solution				Scaffold-pretreated solution
		PLGA amount (mg)	PLA amount (mg)	0.3%w/v Vanco-mycin** (μL)	Dichloro-methane (μL)	0.3%w/v Vanco-mycin** (μL)
1	V-PLGA20-Lvanc	200	–	100	900	400
2	V-PLGA40-Lvanc	400	–	100	900	400
3	V-PLA20-Lvanc	–	200	100	900	400
4	V-PLA40-Lvanc	–	400	100	900	400
5	PLGA20-Lvanc	200	–	–	1000	400
6	PLGA40-Lvanc	400	–	–	1000	400
7	PLA20-Lvanc	–	200	–	1000	400
8	PLA40-Lvanc	–	400	–	1000	400
9	PLGA20-Hvanc	200	–	–	1000	800
10	PLGA40-Hvanc	400	–	–	1000	800
11	PLA20-Hvanc	–	200	–	1000	800
12	PLA40-Hvanc	–	400	–	1000	800

*Formulation codename: (vancomycin blend with the polymer mixture)-(polymer type, concentration %w/v)-(low or high concentration of vancomycin on the scaffold core)
**Vancomycin 0.3%*w/v* was prepared using methanol as solvent.

2.6. Antibiotic-coated/ antibiotic-loaded scaffold physical characterization

The antibiotic-coated/ antibiotic-loaded scaffolds were weight before and after coating via an analytical balance (CP225D, Sartorius, Germany). The surface morphology of uncoated and antibiotic-coated/ antibiotic-loaded scaffolds was observed using the scanning electron microscope (SEM). The samples were mounted on the stubs and then coated with gold by a sputter coater (Blazers SCD 040, Bal-Tec AG, Blazers, Liechtenstein). The images were captured using JSM-6610 LV InTouchScope™ (JEOL, Tokyo, Japan) at 15.0 kV accelerating voltage with low magnification (20×).

2.7. Determination of antibacterial property

The antibacterial property of the PBS-containing antibiotics obtained from the drug elution assay was determined using an agar disc diffusion (Kirby-Bauer) method. The protocol was based on the M100 Performance standards for antimicrobial susceptibility test, The Clinical and Laboratory Standards Institute (CLSI) guidelines, 30th edition. The PBS-containing antibiotics from three time periods in the drug elusion assay (1 h, 24 h, and day 14) were analyzed. The tested paper discs containing 20 μL samples were placed on Mueller Hinton Agar (Difco™, Maryland, USA). *S. aureus* ATCC® 25923 and methicillin-resistant *S. aureus* (MRSA DMST 20654) were used as standard microorganisms for quality control of the tests in a density of approximately 1.5×10^8 CFU/mL. The agar plates were then incubated at 35 ± 2 °C for 16–20 h. The results were interpreted as sensitivity based on the inhibitory zone diameters (mm) around the discs. Each plate contained 5 tested papers, three of the tested samples, one negative control (20 μL of PBS), and one positive control (standard vancomycin 30 μg disc, Lot no. 2927437, Oxoid, UK).

2.8. In vitro cytotoxicity assay

In this set of experiments, the human osteosarcoma cell line (Saos-2, ATCC HTB-85™) was used. Cells were maintained in Dulbecco's Modified Eagle's Medium (DMEM, Gibco®, Life Technologies, USA) supplemented with 10% fetal bovine serum (FBS, triple 0.1 μm sterile filtered, Hyclone™, GE Healthcare Bio-Sciences, Austria) and 1% penicillin/streptomycin (Gibco®). Cells were incubated at 37 °C and 5% CO_2. The handling and subculturing procedures were conducted according to ATCC recommendations with a subcultivation ratio of 1:2 to 1:4.

The in vitro cytotoxicity was conducted based on ISO 10993-5, Biological evaluation of medical devices, 3rd Edition, with some modifications. The treatments in the experiments were the PBS-containing antibiotics obtained at 1 h, 24 h, day 7, and day 14 incubation period in the drug elution assay. Thus, according to ISO 10993-5, the extraction vehicle was PBS (physiological saline solution and the extraction conditions were different incubation periods at 37 °C.

Saos-2 cells were plated one day before the treatment in 96-well plates at a concentration of 1×10^4 cells per well. Cells were exposed to the treatments with the volume ratio of treatment: medium equal to 1:1 (working volume is equal to 100 μL) for 24 and 48 h. At the end of the indicated incubation period, the treatment in each well was replaced with the MTT reagent (PanReac AppliChem ITW Reagents, Spain) in the serum-free medium at the concentration of 0.5 mg/mL. After 2 h, the MTT reagent was replaced with dimethyl sulfoxide (DMSO, Sigma-Aldrich, USA). The absorbance was recorded at 570 nm using a microplate reader. PBS was used as a negative control. Cell viability was determined as a percentage of the absorbance value of cells that were treated with PBS. All absorbance values were adjusted with a blank solution containing 100 μL of DMSO.

2.9. Statistical analysis

Data in graphical format are expressed as mean ± standard error of the mean (SEM). The statistical significance for the cell viability was performed using Two-way ANOVA with Dunnett multiple comparisons test to compare each type of coating with PBS-treated cells. The statistical significance of the scaffold weight variation was determined using Two-way ANOVA with Tukey multiple comparisons test to compare the mean difference in the same coating group, before coating, after coating, and after the drug elution assay. All statistical tests were performed using GraphPad Prism version 7.00 (GraphPad Software, CA, USA, www.graphpad.com). A p-value <0.05 was considered significant.

3. Results

3.1. Hydroxyapatite powder and hydroxyapatite scaffold fabrication

In this study, HAp powder was obtained from the Nile tilapia and used for scaffold fabrication. The HAp scaffolds were fabricated using the P.U. sponge replication technique to obtain scaffolds with 1.2 cm in diameter (Fig. 1A) and 0.4 cm in thickness (Fig. 1B). The average weight of the scaffold was equal to 184 ± 23 mg (mean ± S.D., $n = 40$).

3.2. Hydroxyapatite powder and hydroxyapatite scaffold characterization at the nanostructure level

Hydroxyapatite obtained from the Nile tilapia bones was characterized in the form of powder and scaffolds using XRF, XRD, and FT-IR. The element composition of HAp powder was analyzed via XRF. According to Table 2, the HAp powder obtained from fish bone has calcium (Ca) and phosphorus (P) as the main elements. They have some trace elements, which are magnesium (Mg), sodium (Na), chlorine (Cl), potassium (K), strontium (Sr), silicon (Si), Zinc (Zn), and sulfur (S). These elements were the same elements found in human bones and teeth. Moreover, the calcium-to-phosphate ratio (Ca/P) was equal to 1.63, which is close to the perfect hydroxyapatite ratio (1.67) (Goto and Sasaki, 2014; Ishikawa et al., 1993). Thus, this HAp powder extracted from the Nile tilapia bones is suitable to be used as a scaffold starting material.

Fig. 2 represents FT-IR spectra obtained from the HAp powder and the HAp scaffold (Fig. 2). The characteristic vibrations of hydroxyapatite at 3572, 1024, 964, 630, 600, and 564 cm^{-1} were revealed in both samples (Reyes-Gasga et al., 2013; Ślósarczyk et al., 2005; Shaltout et al., 2011). There are two carbonate-substituted at the hydroxyl site (A-type) and phosphate site (B-type) of hydroxyapatite structure and carbonate group at the surface of the HAp powder (Benataya et al., 2020; Nowicki et al., 2020). However, A-and B-types disappear in the scaffold. The small band at 946 and 984 cm^{-1} indicate the presence of β-TCP and Mg-substituted beta-tricalcium phosphate (β-MgTCP) in the HAp powder and scaffold (Benataya et al., 2020; Nowicki et al., 2020; Cacciotti et al., 2009; Butler and Shahack-Gross, 2017). In addition, no vibration peak of polyurethane was observed. This indicates that the P. U. sponge was completely removed after the sintering process.

Using the XRD, the quantitative phase analyses obtained from the Rietveld refinement method are shown in Fig. 3. The fittings revealed well converged between the experimental and calculated data with the nice goodness of fit (GOF) values of 2.92 and 2.04 for HAp powder and scaffold, respectively. Refinement parameters are also reported with excellent values; $R_{exp} = 2.22$, $R_p = 2.81$, $R_{wp} = 3.97$ for HAp powder and $R_{exp} = 5.28$, $R_p = 5.88$, $R_{wp} = 7.54$ for scaffold. The results showed that the powder contains 91.60% of hydroxyapatite, 8.40% of β-TCP (Fig. 3A). Interestingly, the content of the β-TCP phase increased (13.60%) and the α-TCP (12.50%) was observed after sintering at 1400 °C for 5 h while that of the hydroxyapatite phase (73.90%) decreased (Fig. 3B). This suggests the phase transformation from hydroxyapatite to TCP (Khamkongkaeo et al., 2021), which is consistent

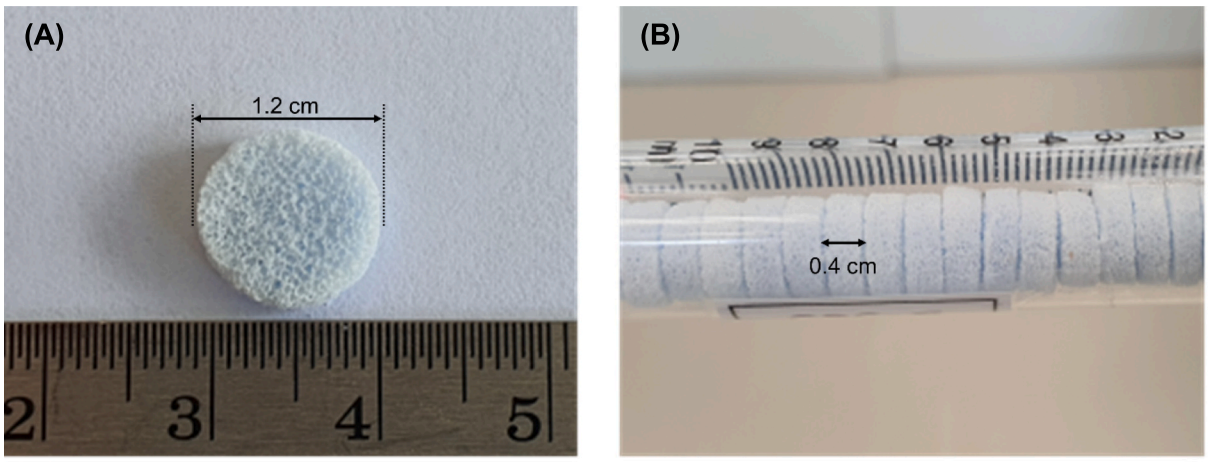

Fig. 1. The hydroxyapatite scaffold fabricated from the Nile tilapia bones. The scaffolds have a diameter equal to 1.2 cm (A) with 0.4 cm thickness (B).

Table 2
The composition in hydroxyapatite powder obtained from the X-ray fluorescence spectroscopy, (XRF).

Elements	Amount		Elements	Amount	
	%*w*/w	at.%		%w/w	at.%
Calcium (Ca)	34.7	31.26	Potassium (K)	0.19	0.18
Phosphorus (P)	16.4	19.12	Strontium (Sr)	0.05	0.02
Magnesium (Mg)	0.66	0.98	Silicon (Si)	0.02	0.02
Sodium (Na)	0.78	1.22	Zinc (Zn)	0.02	0.01
Chlorine (Cl)	0.07	0.07	Sulfur (S)	0.04	0.04
Other elements*	Balanced	Balanced			

* Other elements such as carbon (C), oxygen (O), and hydrogen (H).

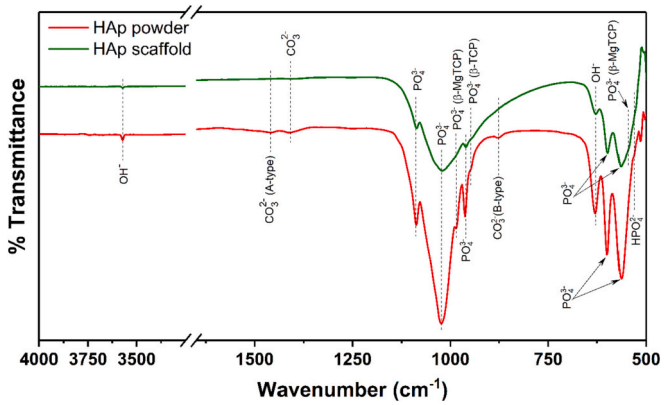

Fig. 2. FT-IR spectra of the HAp powder (red) and HAp scaffold (green) in the wavenumber ranging from 4000 to 500 cm^{-1}. (For interpretation of the references to color in this figure legend, the reader is referred to the web version of this article.)

with the FT-IR results. Furthermore, more crystallographic information, including lattice parameters and atomic coordinates, is reported in the supplementary section (Table S1).

From all the above, it was found that the HAp powder made from the Nile tilapia bones has elements identical to human bones. This HAp powder is suitable as a starting material to build scaffolds. After the scaffold fabrication, the ratio of HAp and β-TCP changed, and the phase transformation of β-TCP to α-TCP was observed. Moreover, the incorporation of Mg in the β -TCP structure of the HAp scaffold may not have a toxic effect on the cells, and it is important for the solubility properties and biological performance of the obtained scaffold (Ressler et al., 2021). In addition, no P.U. residue remains after the sinister. Thus, the P.U.sponge replication technique is suitable for building scaffolds extracted from the Nile tilapia bones. Furthermore, the HAp scaffolds

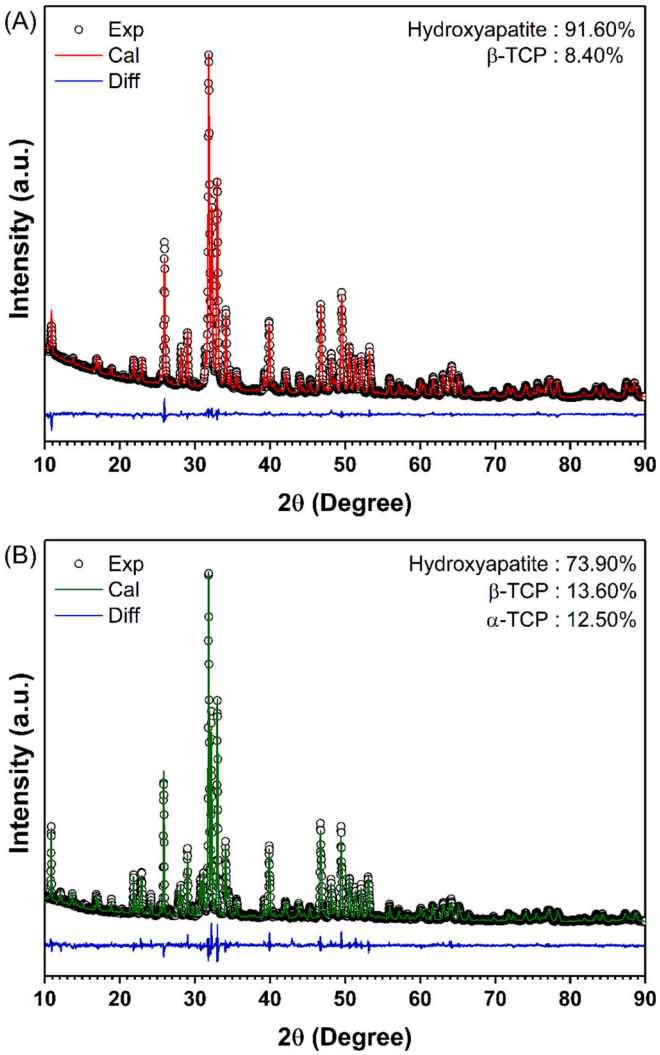

Fig. 3. Rietveld structure refinement plot for the hydroxyapatite powder (A) and the hydroxyapatite scaffold (B). Data was obtained from XRD in the 2θ of 10–90°.

obtained were high quality and suitable for biomedical applications.

3.3. The antibiotic-coated/antibiotic-loaded scaffold formulations

This study prepared three sets (12 formulations, 4 formulations per set) of antibiotic-coated/ antibiotic-loaded scaffolds. Details of all formulations were shown in Table 1. The formulation codename is divided into three parts. 1) *V* represents the formulation with *v*ancomycin blended in the polymer coating solution. 2) PLGA20 or PLGA40 are the formulations with PLGA as a coating solution at 20%*w/v* or 40%w/v, respectively. PLA20 or PLA40 is the formulation with PLA as a coating solution at the concentration of 20%*w/v* or 40%w/v, respectively. 3) Lvanc represents the low vancomycin amount loaded into the scaffold. Hvanc represents the high vancomycin amount that was loaded into the scaffold.

On the first set (Formulation 1–4), 400 μL of 0.3%*w/v* vancomycin was loaded into the scaffolds. Afterward, the scaffolds were coated with PLGA or PLA containing 0.03%*w/v* vancomycin and 20%*w/v* or 40%w/v of polymer. Thus, Formulation 1–4 would have vancomycin in both the scaffolds and in the coating solution (the antibiotic-coated/ antibiotic-loaded scaffolds).

On the second set (Formulation 5–8), the scaffolds were also loaded with 0.3%w/v vancomycin (400 μL) prior to being coated with the PLGA or PLA at the polymer concentration of 20%w/v or 40%w/v. Formulation 5–8 contained the antibiotic only in the scaffolds but not in the coating (the antibiotic-loaded scaffolds).

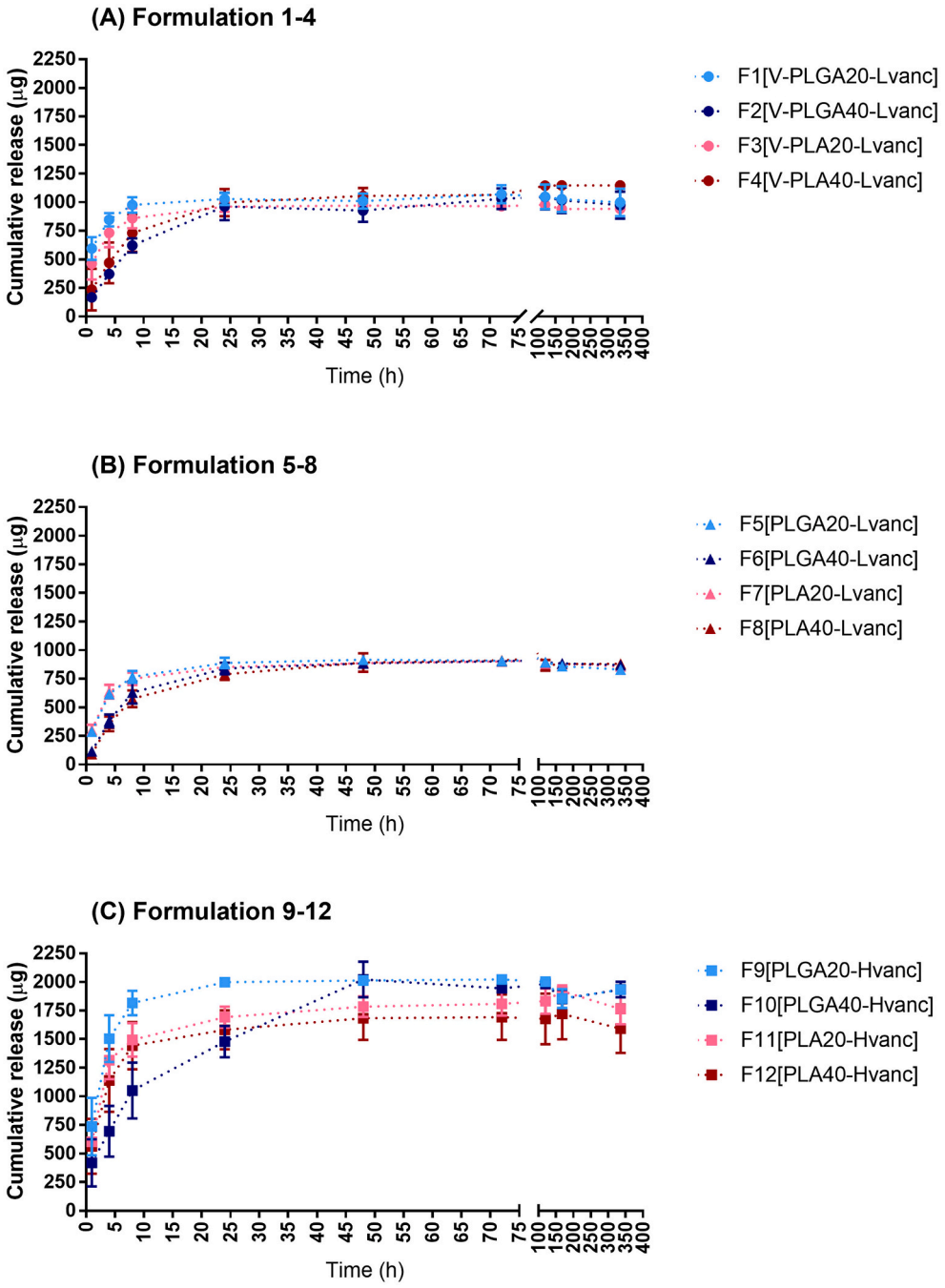

Fig. 4. The cumulative release profiles of vancomycin from the antibiotic-coated scaffold Formulation 1–4 (A), (B), Formulation 5–8 (C), (D), and Formulation 9–12 (E), (F). The vancomycin release was monitored for 14 days. Data are expressed as mean ± SEM.

On the third set (Formulation 9–12), the scaffolds were loaded with 0.3%w/v vancomycin (800 μL) before being coated with the PLGA or PLA (20%w/v or 40%*w/v*). Formulation 9–12 contained the antibiotic only in the scaffolds but not in the coating (the antibiotic-loaded scaffolds). Although the second and third sets had similar coating solutions, Formulation 9–12 had higher vancomycin loaded in the scaffolds than Formulation 5–8. Formulation 9–12 contained the highest amount of drug, followed by Formulation 1–4 and Formulation 5–8, respectively.

3.4. Vancomycin release profiles from the antibiotic-coated/ antibiotic-loaded scaffolds

Fig. 4 represents the cumulative release of vancomycin from the antibiotic-coated/ antibiotic-loaded scaffolds. Three factors were involved in the formulation design; 1) adding vancomycin to the coating solution (comparing between Formulation 1–4 with Formulation 5–8), 2) the amount of vancomycin used in the scaffold pretreatment (comparing between Formulation 5–8: low concentration and Formulation 9–12: high concentration), and 3) the types and concentrations of polymers in the coating solution.

All 12 formulations can release vancomycin from the scaffolds. Most showed a rapid release in the first 72 h before reaching a plateau phase. Formulation 1–4 (Fig. 4A), which contains *v*ancomycin both in the scaffold core and the coating, showed a slightly higher amount and faster drug release profile than Formulation 5–8, with no vancomycin in the coating solution (Fig. 4B). This is especially apparent when comparing F1[*V*-PLGA20-Lvanc] with F5[PLGA20-Lvanc] (Supplementary fig. 2A). Thus, adding vancomycin to the coating solution can increase the drug release and accelerate the drug release into the en*v*ironment.

The amount of vancomycin used in the scaffold pretreatment is strongly associated with the drug release profile. Formulation 9–12, containing 800 μL of 0.3%*w/v* vancomycin, gave the cumulative release of approximately 2000 μg at day 14 (Fig. 4C). Formulation 5–8, containing 400 μL of 0.3%w/v vancomycin, gave the cumulative release of approximately 1000 μg at day 14 (Fig. 4B). Using a high amount of vancomycin gave higher cumulative drug release than using a low amount. However, there is no change in the release profile trend. They all reached a plateau phase within 72 h.

This study used two types of polymers as a coating material: PLGA and PLA, with two concentrations, 20%w/v and 40%w/v. Overall, scaffolds coated with PLGA showed a faster drug release profile than PLA in the first 72 h (Fig. 4A, B, and C). This is as expected. PLGA and PLA are biodegradable polymers. Typically, PLGA copolymers degrade much faster than homopolymers such as PLA. In particular, the PLGA with the ratio of polylactic acid (PLA): poly glycolic acid (PGA) equal to 50:50, which exhibits the fastest degradation, was employed in this study (Makadia and Siegel, 2011a). As a result, the scaffolds coated with PLGA obtained a faster drug release profile than those with PLA coating. Having a low PLGA concentration (Supplementary fig. 2A) in the coating solutions gave a faster drug release profile than a high PLGA concentration (Supplementary fig. 2B). Surprisingly, different coating concentrations in PLA slightly impacted the drug release profile (Supplementary fig. 2C and 2D). This could be the result of the slow degradation of PLA. According to Silva et al. (da Silva et al., 2018), the median half-life of PLA is 30 weeks. Another factor that can be involved is the viscosity of the coating solution. The relationship between PLA coating concentrations and the drug release profile needs further investigation.

3.5. Physical characteristics of the antibiotic-coated/ antibiotic-loaded scaffolds before and after the drug elusion assay

The scaffolds were weight before, after coating, and after 14 days of drug elution assay. Uncoated scaffolds' weight was in the range of 0.176–0.196 g. (mean). After coating, the weight increased to 0.261–0.292 g. (mean). These significant weight changes ($p < 0.001$) came from the coating. Afterward, the antibiotic-coated/ antibiotic-loaded scaffolds were weight again at the end of the drug elution assay. After being incubated in the PBS for 14 days, the scaffolds' weights were slightly reduced compared to the weight after coating but statistically insignificant (Supplementary fig. 3).

The second set of formulation (Formulation 5–9) were chosen to study the surface morphology of the scaffolds before and after the drug elution assay (Fig. 5). There is no difference in the scaffold surface when comparing the antibiotic-loaded scaffolds (Formulation 5–8) and the blank polymer-coated scaffolds (Supplementary Fig. 4). Comparing the freshly coated scaffolds, all formulations (Fig. 5A, C, E, and G) showed the coating as seen by the different surface morphology when compared to the blank (uncoated) scaffold (Fig. 5I). PLA coating (F7[PLA20-L*v*anc] (Fig. 5E) and F8[PLA40-Lvanc] (Fig. 5G)) gave thicker surface than PLGA coating (F5[PLGA20-Lvanc] and F6[PLGA40-Lvanc]). Moreover, comparing the same type of polymer, an increase in the PLGA concentration from 20%*w/v* (F5[PLGA20-Lvanc], Fig. 5A) to 40%w/v (F6 [PLGA40-Lvanc], Fig. 5C) resulted in a thicker coating. However, this difference was not clearly seen in the PLA group. Increasing the PLA concentration from 20%w/v (F7[PLA20-Lvanc), Fig. 5E) to 40%w/v (F8 [PLA40-Lvanc], Fig. 5G) had a slightly or no effect on coating thickness.

After 14 days in the PBS solution, no change was observed using SEM in the blank scaffold group (Fig. 5J). However, all antibiotic-coated/ antibiotic-loaded scaffolds showed a trace of erosion (Fig. 5B, D, F, and H). This is consistent with the drug elution assay that all samples can release vancomycin into the environment.

3.6. Antibacterial activities of the antibiotic-coated/ antibiotic-loaded scaffolds

The antimicrobial properties of antibiotic-coated/ antibiotic-loaded scaffolds were tested against *S. aureus* and MRSA since both are the most common pathogen in orthopaedic infections (Latha et al., 2019; Chen et al., 2013). The experiments were conducted using the PBS-containing antibiotic solutions (supernatant) obtained from 3 designated time points (1 h, 24 h, and day 14) during the drug elution assay (Fig. 6). When comparing the bacterial types, the PBS-containing antibiotic solutions ga*v*e a larger inhibition zone in *S. aureus* treated than in MRSA treated. *S. aureus* is more susceptible to vancomycin than MRSA. When comparing formulations, pretreating the scaffold with high vancomycin concentration (Fig. 6C and D) resulted in a larger inhibition zone than the scaffolds that were pretreated with low vancomycin concentration (Fig. 6A and B).

All formulations can inhibit *S. aureus* in all time points, except F6 [PLGA40-Lvanc] at 1 h (Fig. 6A) and F10[PLGA40-Hvanc] at 1 h (Fig. 6C). This could come from the low amount of drug release at the beginning of the drug elution assay (Fig. 4D and F). The result is consistent with the drug elusion assay that scaffolds coated with PLGA 20%*w/v* can release vancomycin faster than the scaffolds coated with PLGA 40%w/v. The inhibition zone at 24 h was the largest among the same coating groups. On day 14, Although the cumulative vancomycin release is not reduced (Fig. 4A, C, and E), the actual concentration inside the centrifugation tube is reduced by sampling the solution repeatedly at each designated time point. Thus, it is possible that the inhibition zone on day 14 was smaller than 24 h.

MRSA results follow the same trend as *S. aureus*, except some formulations cannot exhibit antibacterial activity on day 1 and day 14 (Fig. 6B and D). F6[PLGA40-Lvanc] showed no inhibition zone at 1 h, which is consistent with the result from *S. aureus*. F7[PLA20-Lvanc] and F8[PLA40-Lvanc] showed no sign of inhibition on day 14. This could be due to the low vancomycin concentration after sampling the solution many times.

3.7. In vitro cell cytotoxicity

The possible cytotoxicity of the antibiotic-coated/ antibiotic-loaded

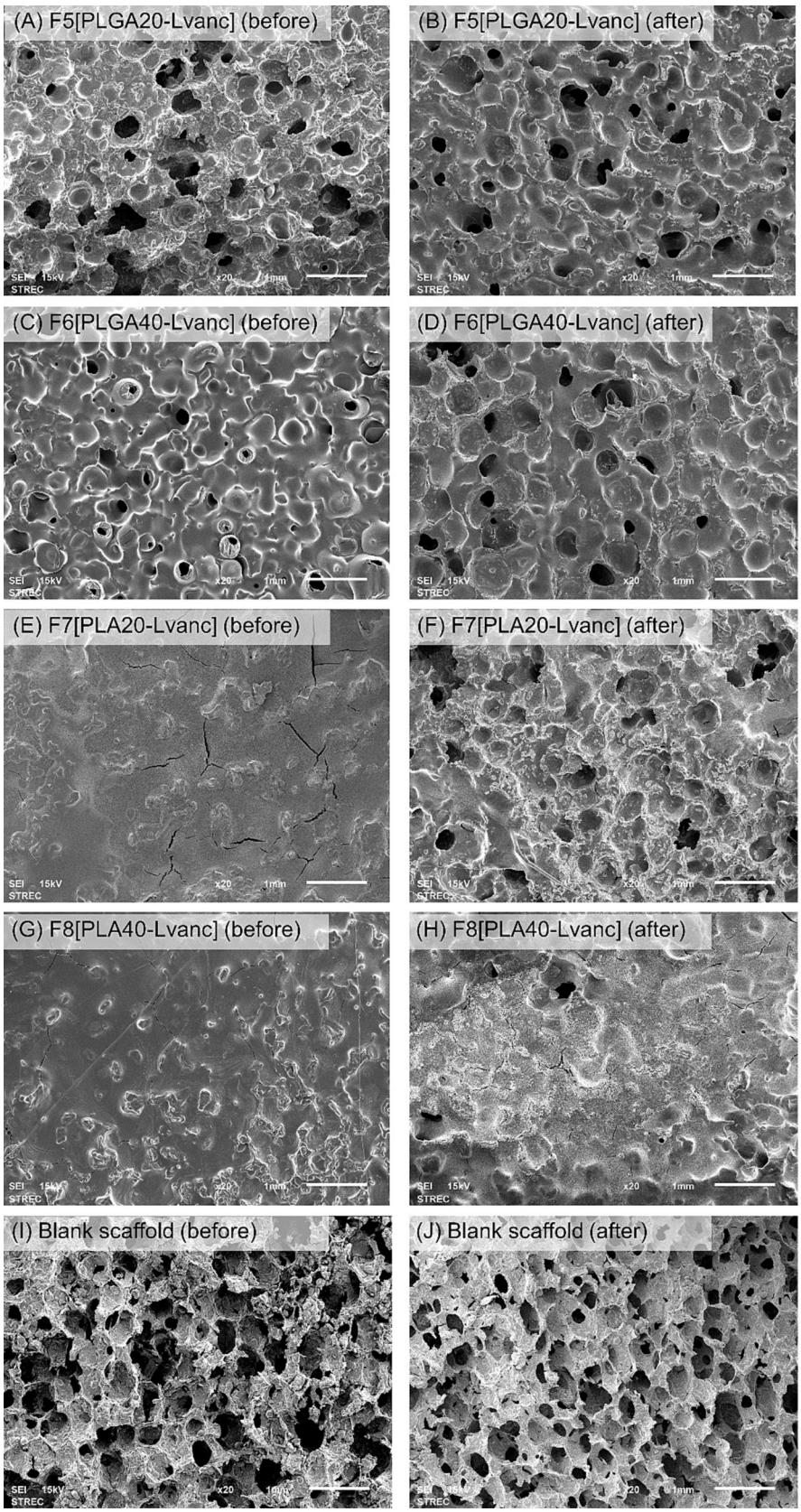

Fig. 5. SEM micrographs represent antibiotic-coated/ antibiotic-loaded scaffolds (Formulation 5–8) obtained fresh after coating (A, C, E, G) and after submerged in PBS for 14 days (B, D, F, H). Blank or uncoated scaffold before (I) and after the submersion (J) are shown. Images were taken at 20× magnification. Scale bar represents 1 mm.

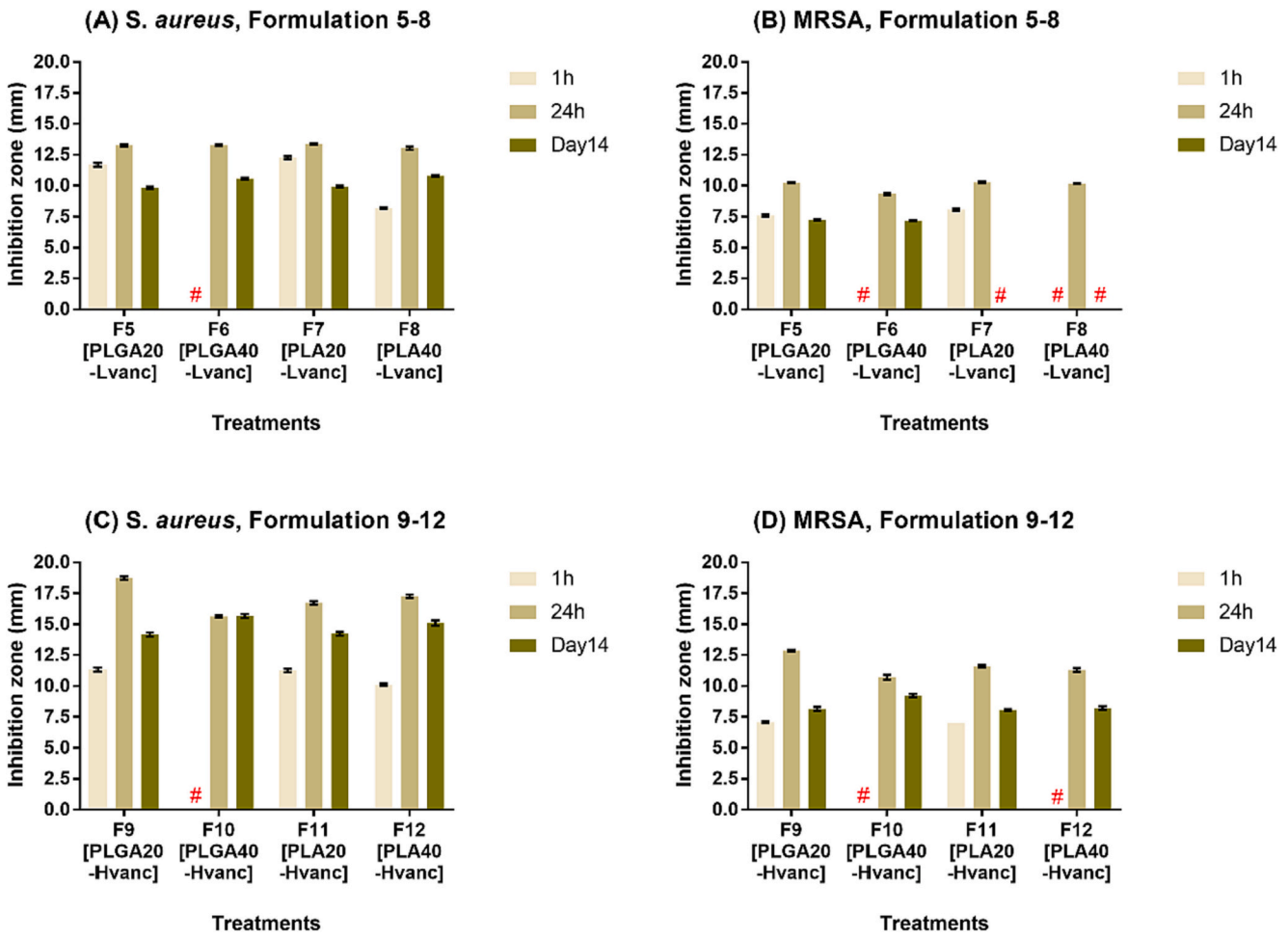

Fig. 6. Inhibition zone of *S. aureus* (A, C) and MRSA (B, D) of the PBS containing antibiotic solution obtained from 8 different scaffold formulations (Formulation 5–8, A-B and Formulation 9–12, C—D) that incubated in PBS for 1 h, 24 h, and 14 days. Data are expressed as mean ± SEM. # represents no inhibition zone (0 mm).

scaffolds and their degradation products were assessed via an MTT assay. The PBS-containing antibiotic collected from the drug elution assays (the extracts) at 4 different time points (1 h, 24 h, day 7, and day 14) were studied. Saos-2 cells were exposed to the treatments for 24 h. Two sets of formulations, which are low vancomycin concentration (Formulation 5–8, Fig. 7A) and high vancomycin concentration (Formulation 9–12, Fig. 7B), showed relative cell viability (%) higher than 70. It can be concluded that all antibiotics-coated/ antibiotic-loaded scaffolds and their possible degraded products showed no sign of cytotoxicity according to ISO 10993-5. In all cytotoxicity tests, sodium lauryl sulfate (SLS) was used as a positive control with 6 concentrations ranging from 6.25 to 200 μg/mL to confirm the reliability of the result (Fig. 7D).

The cell viability in various formulations on day 7 and day 14 showed a very high % cell viability ($p < 0.001$). According to Fig. 7C, the blank scaffold can accelerate Saos-2 cell growth (≥ 200%) after being eluted in PBS for 24 h, day 7, and day 14. The surface of HAp scaffolds degraded and released HAp into the PBS solution. HAp found in the PBS solution can activate Saos-2 cell growth. This is consistent with the work by Wee et al. that HAp microparticles can degrade in physiological conditions (Wee et al., 2022).

Cell viability from the extracts incubated with blank scaffolds for 24 h can stimulate cell growth (Fig. 7C). However, cells that were treated with the extracts incubated with antibiotic-coated/ antibiotic-loaded scaffolds for 24 h showed no sign of cell growth beyond the PBS-treated group (Fig. 7A and B). It is possible that coating the scaffold with antibiotic and polymer gives a shielding effect, protects the HAp surface from erosion, and retard the HAp release to the medium.

The HAp scaffolds made from the Nile tilapia bones can stimulate bone cell growth. This result was consistent with previous studies using HAp from various sources. Sari et al. (Sari et al., 2021) synthesized the HAp scaffolds from abalone mussel shells and found that the scaffolds can facilitate the attachment of MC3T3-E1 bone cells. Surya et al. (Surya et al., 2021) fabricated the HAp in the form of nano-HAp from fish bone (*Sardinella longiceps*). This nano-HAp can increase the cell viability of the human osteoblast bone cells (MG-63) to 140% at a concentration of 100 μg/mL (Surya et al., 2021). Guarino et al. found that adding HAp particles into the polymeric scaffolds enhances the scaffold bioactivity and osteoblast cell response (Guarino et al., 2009).

4. Discussion

According to this study, it was found that the HAp powder made from the Nile tilapia bones has elements identical to human bones. This HAp powder is suitable as a starting material to build scaffolds. After the scaffold fabrication, the ratio of HAp to β-TCP changed, and the phase transformation of β-TCP to α-TCP was observed. The increased β-TCP in the scaffolds can benefit bone cells. β-TCP is one of the most potent bone graft substitutes because of its biocompatibility, osteoconductive and osteoinductive properties (Bohner et al., 2020; Tang et al., 2017). Reports suggest that β-TCP has better osteoinductivity than HAp (Hou et al., 2022). Ogose et al. compare β-TCP and HAp as bone substitutes after bone tumor excision in 23 patients. It was found that the β-TCP gave better bone remodeling results and superior osteoconductivity than

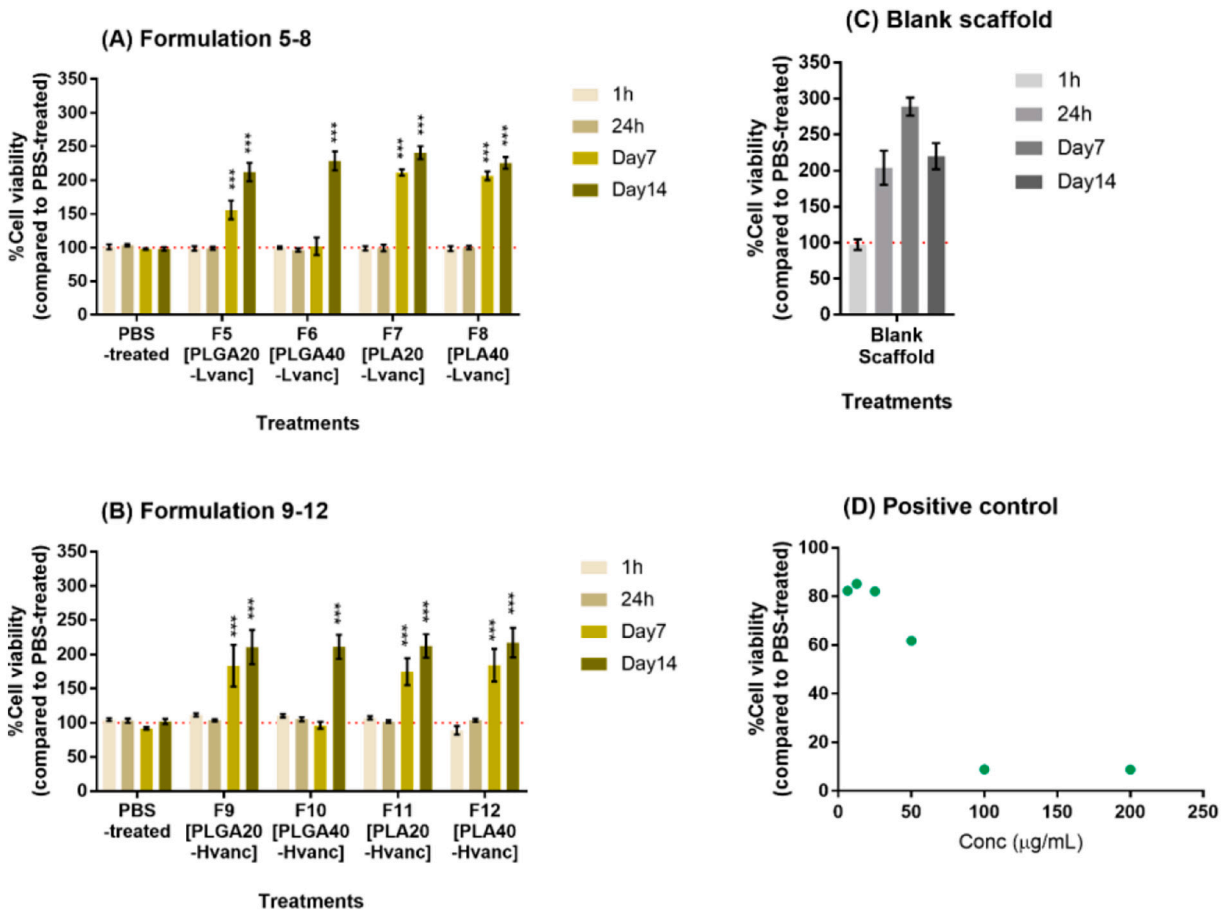

Fig. 7. Relative cell viability (%) of Saos-2 cells after treated with the PBS-containing antibiotic solution for 24 h. The PBS-containing antibiotic solutions obtained from the drug elution assay using different scaffold formulations (Formulation 5–8, A; Formulation 9–12, B). The PBS extracted from blank (untreated) scaffolds were also tested (C). SLS concentration ranging from 6.25 μg/mL to 200 μg/mL was used as a positive control in all experiments (D). Data are expressed as mean ± SEM. Two-way ANOVA with Dunnett multiple comparisons test was performed. ***$p < 0.001$.

HAp (Ogose et al., 2005).

From the FT-IR results, no P.U. residue remains after the sinister. Thus, the P.U.sponge replication technique is suitable for building scaffolds extracted from the Nile tilapia bones. Furthermore, the HAp scaffolds obtained were of high quality and suitable for biomedical applications.

These experimental sets showed that the antibiotic release profile could be tailored by adding antibiotic(s) in the coating, adjusting the amount of the drug in the scaffold as a pretreatment, and changing the polymer type/concentration in the coating solution. Besides all these factors, there are other variables. Since PLGA and PLA are degraded through the hydrolysis of the polyester backbone, the surface area exposed to the liquid environment plays an important role. The size of pores inside the scaffold, pore number per volume, and the interporeconnectivity of the 3D structure (tortuosity) directly affect the surface area and, therefore, the drug release kinetics (Rambhia and Ma, 2015).

To build a scaffold, the mechanical property is also another factor to consider. The mechanical properties of these scaffolds are typically measured using the standard test method used for compressive properties of rigid plastics (ASTM D695–15) (ASTM S. D695, 2008). The standard test specimen must have a specific shape, length, and be cylindrical. On the other hand, the HAp scaffold in our study was designed in a coin shape. As a result, they are ineligible for mechanical property testing. It is well-known that HAp has poor mechanical properties. It has low tensile strength with low compressive strength (Ielo et al., 2022). There are reports suggesting that HAp mechanical properties can be improved by blending or coating polymers. According to Guo et al., coating PLA on HAp nanowires can improve mechanical performance (Guo et al., 2020). Zusho et al. found that coating PLA on HAp scaffolds can increase Young's modulus and compressive strength (Zusho et al., 2020). Coating the scaffolds with PLGA can reinforce the scaffold strength but not as much as PLA (Guo et al., 2020).

Correlating the in vitro drug release to the in vivo drug profiles is always challenging in pharmaceutical development. In this study, most vancomycin was released in the first 72 h. These release rates at the in vitro level may not fully reflect the drug release in humans. Although the polymer degradation rate dictates the drug release kinetics, other factors are involved. The drug elution study was conducted in the shaking incubator where the surrounding liquid offered a sink condition, and the stagnant layer was thin (Frenning, 2011). In the human body, scaffolds may be exposed to limited amounts of exudate with low liquid exchange rates. Moreover, enzymatic degradation may play a role in the PLGA and PLA degradation mechanisms (Makadia and Siegel, 2011b). These factors may alter the drug release rate in humans.

The amount of vancomycin released plays a vital role in the antibacterial effect. In this study, all formulations with high vancomycin concentrations can inhibit *S. aureus* and MRSA at all designated time points. In contrast, some samples obtained from the low vancomycin concentration formulations can inhibit bacteria, and some cannot. In the drug elution assay, the PBS volume was fixed at 30 mL. However, in the actual circumstance, the wound exudate or the wound drainage volume is an uncontrollable factor. It depends on the severity of the wound and infection, the surgical site, and surgical techniques. These factors must be considered when developing antibiotic(s)-coated/ antibiotic-loaded

scaffolds.

5. Conclusions

To the best of our knowledge, this is the first study to show that the HAp powder extracted from the Nile tilapia bones can be fabricated into scaffolds. These HAp scaffolds have positive effects on bone cells. These fish bones considered waste products, can potentially be converted into raw material for biomedical applications in the near future. Besides the scaffold core, the antibiotic-coating scaffolds were developed with 12 different formulations. The antibiotic release rate could be tailored using different polymer types and concentrations and by varying the amount of antibiotic inside the coating solution and the scaffold core. These scaffolds can inhibit bacterial growth with no sign of cytotoxicity to bone cells.

Ethics approval and consent to participate

All experiment sets in the study above were only related to in vitro experiments. There is no animals or human involved. As such, there is no need for any ethical declaration.

Funding

This research paper is supported by Specific League Funds from Mahidol University. The funding body has no role in the study design, collection, analysis, and interpretation of the data. The funding body also has no role in writing this manuscript.

CRediT authorship contribution statement

Atchara Khamkongkaeo: Conceptualization, Data curation, Formal analysis, Investigation, Methodology, Project administration, Validation, Visualization, Writing – original draft, Writing – review & editing. **Arreerat Jiamprasertboon:** Data curation, Methodology. **Nanthawan Jinakul:** Data curation, Methodology, Conceptualization, Writing - review & editing. **Phatraya Srabua:** Data curation, Methodology. **Saran Tantavisut:** Conceptualization, Formal analysis, Investigation, Validation, Writing – review & editing. **Amaraporn Wongrakpanich:** Conceptualization, Data curation, Formal analysis, Funding acquisition, Investigation, Methodology, Project administration, Supervision, Validation, Visualization, Writing – original draft, Writing – review & editing.

Declaration of Competing Interest

All authors declare no financial or non-financial competing interests.

Data availability

Data will be made available on request.

Acknowledgments

The authors would like to thank Ms. Awadsaya Pakdee and Ms. Nattika Khamkhantee for the lab technical support.

Appendix A. Supplementary data

Supplementary data to this article can be found online at https://doi.org/10.1016/j.ijpx.2023.100169.

References

Agarwal, S., Morshed, M., Labour, M.-N., Hoey, D., Duffy, B., Curtin, J., et al., 2016. Enhanced corrosion protection and biocompatibility of a PLGA–silane coating on AZ31 Mg alloy for orthopaedic applications. RSC Adv. 6 (115), 113871–113883.
ASTM S. D695, 2008. Standard Test Method for Compressive Properties of Rigid Plastics. ASTM International, West Conchohocken.
Baertl, S., Metsemakers, W.-J., Morgenstern, M., Alt, V., Richards, R.G., Moriarty, T.F., et al., 2021. Fracture-related infection. Bone Joint Res. 10 (6), 351–353.
Benataya, K., Lakrat, M., Elansari, L.L., Mejdoubi, E., 2020. Synthesis of B-type carbonated hydroxyapatite by a new dissolution-precipitation method. Mater. Today: Proc. 31. S83-S8.
Bernardo, M.P., da Silva, B.C.R., Hamouda, A.E.I., de Toledo, M.A.S., Schalla, C., Rütten, S., et al., 2022. PLA/Hydroxyapatite scaffolds exhibit in vitro immunological inertness and promote robust osteogenic differentiation of human mesenchymal stem cells without osteogenic stimuli. Sci. Rep. 12 (1), 2333.
Bohner, M., Santoni, B.L.G., Döbelin, N., 2020. β-Tricalcium phosphate for bone substitution: Synthesis and properties. Acta Biomater. 113, 23–41.
Bouffi, C., Thomas, O., Bony, C., Giteau, A., Venier-Julienne, M.-C., Jorgensen, C., et al., 2010. The role of pharmacologically active microcarriers releasing TGF-β3 in cartilage formation in vivo by mesenchymal stem cells. Biomaterials. 31 (25), 6485–6493.
Butler, D.H., Shahack-Gross, R., 2017. Formation of biphasic hydroxylapatite-beta magnesium tricalcium phosphate in heat treated salmonid vertebrae. Sci. Rep. 7 (1), 3610.
Cacciotti, I., Bianco, A., Lombardi, M., Montanaro, L., 2009. Mg-substituted hydroxyapatite nanopowders: Synthesis, thermal stability and sintering behaviour. J. Eur. Ceram. Soc. 29 (14), 2969–2978.
Chen, A.F., Wessel, C.B., Rao, N., 2013. Staphylococcus aureus screening and decolonization in orthopaedic surgery and reduction of surgical site infections. Clin. Orthop. Relat. Res. 471 (7), 2383–2399.
da Silva, D., Kaduri, M., Poley, M., Adir, O., Krinsky, N., Shainsky-Roitman, J., et al., 2018. Biocompatibility, biodegradation and excretion of polylactic acid (PLA) in medical implants and theranostic systems. Chem. Eng. J. 340, 9–14.
Depypere, M., Morgenstern, M., Kuehl, R., Senneville, E., Moriarty, T.F., Obremskey, W. T., et al., 2020. Pathogenesis and management of fracture-related infection. Clin. Microbiol. Infect. 26 (5), 572–578.
Feng, P., Wu, P., Gao, C., Yang, Y., Guo, W., Yang, W., et al., 2018. A multimaterial scaffold with tunable properties: toward bone tissue repair. Adv. Sci. 5 (6), 1700817.
Feng, P., Wang, K., Shuai, Y., Peng, S., Hu, Y., Shuai, C., 2022. Hydroxyapatite nanoparticles in situ grown on carbon nanotube as a reinforcement for poly (ε-caprolactone) bone scaffold. Mater. Today Adv. 15, 100272.
Firdaus Hussin, M.S., Abdullah, H.Z., Idris, M.I., Abdul Wahap, M.A., 2022. Extraction of natural hydroxyapatite for biomedical applications—a review. Heliyon. 8 (8), e10356.
Foster, A.L., Moriarty, T.F., Trampuz, A., Jaiprakash, A., Burch, M.A., Crawford, R., et al., 2020a. Fracture-related infection: current methods for prevention and treatment. Expert Rev. Anti-Infect. Ther. 18 (4), 307–321.
Foster, A.L., Moriarty, T.F., Trampuz, A., Jaiprakash, A., Burch, M.A., Crawford, R., et al., 2020b. Fracture-related infection: current methods for prevention and treatment. Expert Rev. Anti-Infect. Ther. 18 (4), 307–321.
Frenning, G., 2011. Modelling drug release from inert matrix systems: from moving-boundary to continuous-field descriptions. Int. J. Pharm. 418 (1), 88–99.
Goto, T., Sasaki, K., 2014. Effects of trace elements in fish bones on crystal characteristics of hydroxyapatite obtained by calcination. Ceram. Int. 40 (7, Part B), 10777-85.
Granito, R.N., Muniz Renno, A.C., Yamamura, H., de Almeida, M.C., Menin Ruiz, P.L., Ribeiro, D.A., 2018. Hydroxyapatite from fish for Bone Tissue Engineering: a Promising Approach. Int. J. Mol. Cell Med. 7 (2), 80–90.
Guarino, V., Taddei, P., Foggia, M., Fagnano, C., Ciapetti, G., Ambrosio, L., 2009. The influence of hydroxyapatite particles on in vitro degradation behavior of poly ε-caprolactone–based composite scaffolds. Tissue Eng. A 15, 3655–68.
Guo, L., Du, Z., Wang, Y., Cai, Q., Yang, X., 2020. Degradation behaviors of three-dimensional hydroxyapatite fibrous scaffolds stabilized by different biodegradable polymers. Ceram. Int. 46 (9), 14124–14133.
Hadi, H., 2014. Spectrophotometric determination of vancomycin hydrochloride in pharmaceutical preparations through diazotization and coupling reactions. Iraqi J. Sci. 55 (4B), 1684–1693.
Hou, X., Zhang, L., Zhou, Z., Luo, X., Wang, T., Zhao, X., et al., 2022. Calcium Phosphate-based Biomaterials for Bone Repair. J. Funct. Biomater. 13 (4), 187.
Ielo, I., Calabrese, G., De Luca, G., Conoci, S., 2022. Recent advances in hydroxyapatite-based biocomposites for bone tissue regeneration in orthopedics. Int. J. Mol. Sci. 23 (17), 9721.
Ishikawa, K., Ducheyne, P., Radin, S., 1993. Determination of the Ca/P ratio in calcium-deficient hydroxyapatite using X-ray diffraction analysis. J. Mater. Sci. Mater. Med. 4 (2), 165–168.
Khamkongkaeo, A., Boonchuduang, T., Klysubun, W., Amonpattaratkit, P., Ht, Chunate, Tuchinda, N., et al., 2021. Sintering behavior and mechanical properties of hydroxyapatite ceramics prepared from Nile Tilapia (Oreochromis niloticus) bone and commercial powder for biomedical applications. Ceram. Int. 47 (24), 34575–34584.
Latha, T., Anil, B., Manjunatha, H., Chiranjay, M., Elsa, D., Baby, N., et al., 2019. MRSA: the leading pathogen of orthopedic infection in a tertiary care hospital, South India. Afr. Health Sci. 19 (1), 1393–1401.
Makadia, H.K., Siegel, S.J., 2011a. Poly lactic-co-glycolic acid (PLGA) as biodegradable controlled drug delivery carrier. Polymers (Basel) 3 (3), 1377–1397.

Makadia, H.K., Siegel, S.J., 2011b. Poly lactic-co-glycolic acid (PLGA) as biodegradable controlled drug delivery carrier. Polymers. 3 (3), 1377–1397.
Marliana, A., Fitriani, E., Ramadhan, F., Suhandono, S., Yuliani, K., Windarti, T., 2015. Synthesis and characterization of hydroxyapatite from fish bone waste. AIP Conf. Proc. 1699 (1), 040006.
Meirelles, L., Arvidsson, A., Andersson, M., Kjellin, P., Albrektsson, T., Wennerberg, A., 2008. Nano hydroxyapatite structures influence early bone formation. J. Biomed. Mater. Res. A 87 (2), 299–307.
Mohd Pu'ad, N.A.S., Koshy, P., Abdullah, H.Z., Idris, M.I., Lee, T.C., 2019. Syntheses of hydroxyapatite from natural sources. Heliyon. 5 (5), e01588.
Morgenstern, M., Kühl, R., Eckardt, H., Acklin, Y., Stanic, B., Garcia, M., et al., 2018. Diagnostic challenges and future perspectives in fracture-related infection. Injury. 49 (Suppl. 1), S83–s90.
Narayanan, G., Vernekar, V.N., Kuyinu, E.L., Laurencin, C.T., 2016. Poly (lactic acid)-based biomaterials for orthopaedic regenerative engineering. Adv. Drug Deliv. Rev. 107, 247–276.
Neut, D., van de Belt, H., Stokroos, I., van Horn, J.R., van der Mei, H.C., Busscher, H.J., 2001. Biomaterial-associated infection of gentamicin-loaded PMMA beads in orthopaedic revision surgery. J. Antimicrob. Chemother. 47 (6), 885–891.
Nowicki, D.A., Skakle, J.M.S., Gibson, I.R., 2020. Faster synthesis of A-type carbonated hydroxyapatite powders prepared by high-temperature reaction. Adv. Powder Technol. 31 (8), 3318–3327.
Ogose, A., Hotta, T., Kawashima, H., Kondo, N., Gu, W., Kamura, T., et al., 2005. Comparison of hydroxyapatite and beta tricalcium phosphate as bone substitutes after excision of bone tumors. J Biomed Mater Res B Appl Biomater 72 (1), 94–101.
O'Hare, P., Meenan, B.J., Burke, G.A., Byrne, G., Dowling, D., Hunt, J.A., 2010. Biological responses to hydroxyapatite surfaces deposited via a co-incident microblasting technique. Biomaterials. 31 (3), 515–522.
Oonishi, H., 1991. Orthopaedic applications of hydroxyapatite. Biomaterials. 12 (2), 171–178.
Ortega-Oller, I., Padial-Molina, M., Galindo-Moreno, P., O'Valle, F., Jódar-Reyes, A.B., Peula-García, J.M., 2015. Bone regeneration from PLGA micro-nanoparticles. Biomed. Res. Int. 2015, 415289.
Park, J.S., Lim, H.J., Yi, S.W., Park, K.H., 2016. Stem cell differentiation-related protein-loaded PLGA microspheres as a novel platform micro-typed scaffold for chondrogenesis. Biomed. Mater. 11 (5), 055003.
Patel, M., Jha, A., Patel, R., 2021. Potential application of PLGA microsphere for tissue engineering. J. Polym. Res. 28 (6), 214.
Petit, R., 1999. The use of hydroxyapatite in orthopaedic surgery: a ten-year review. Eur. J. Orthop. Surg. Traumatol. 9 (2), 71–74.
Qiu, X.S., Chen, Y.X., Qi, X.Y., Shi, H.F., Wang, J.F., Xiong, J., 2017. Outcomes of cement beads and cement spacers in the treatment of bone defects associated with post-traumatic osteomyelitis. BMC Musculoskelet. Disord. 18 (1), 256.
Qiu, X.-s., Cheng, B., Chen, Y.-x., Qi, X.-y., Sha, W.-p., Chen, G.-z., 2018. Coating the plate with antibiotic cement to treat early infection after fracture fixation with retention of the implants: a technical note. BMC Musculoskelet. Disord. 19 (1), 360.
Rambhia, K.J., Ma, P.X., 2015. Controlled drug release for tissue engineering. J. Control. Release 219, 119–128.
Ressler, A., Žužić, A., Ivanišević, I., Kamboj, N., Ivanković, H., 2021. Ionic substituted hydroxyapatite for bone regeneration applications: a review. Open Ceram. 6, 100122.
Reyes-Gasga, J., Martínez-Piñeiro, E.L., Rodríguez-Álvarez, G., Tiznado-Orozco, G.E., García-García, R., Brès, E.F., 2013. XRD and FTIR crystallinity indices in sound human tooth enamel and synthetic hydroxyapatite. Mater. Sci. Eng. C 33 (8), 4568–4574.
Sari, M., Hening, P., Chotimah, Ana I.D., Yusuf, Y., 2021. Bioceramic hydroxyapatite-based scaffold with a porous structure using honeycomb as a natural polymeric Porogen for bone tissue engineering. Biomater. Res. 25 (1), 2.
Schmolders, J., Hischebeth, G.T., Friedrich, M.J., Randau, T.M., Wimmer, M.D., Kohlhof, H., et al., 2014. Evidence of MRSE on a gentamicin and vancomycin impregnated polymethyl-methacrylate (PMMA) bone cement spacer after two-stage exchange arthroplasty due to periprosthetic joint infection of the knee. BMC Infect. Dis. 14, 144.
Shaltout, A.A., Allam, M.A., Moharram, M.A., 2011. FTIR spectroscopic, thermal and XRD characterization of hydroxyapatite from new natural sources. Spectrochim. Acta A Mol. Biomol. Spectrosc. 83 (1), 56–60.
Shi, P., Liu, M., Fan, F., Yu, C., Lu, W., Du, M., 2018. Characterization of natural hydroxyapatite originated from fish bone and its biocompatibility with osteoblasts. Mater. Sci. Eng. C 90, 706–712.
Shinsako, K., Okui, Y., Matsuda, Y., Kunimasa, J., Otsuka, M., 2008. Effects of bead size and polymerization in PMMA bone cement on vancomycin release. Biomed. Mater. Eng. 18 (6), 377–385.
Shuai, C., Yang, W., Feng, P., Peng, S., Pan, H., 2021. Accelerated degradation of HAP/PLLA bone scaffold by PGA blending facilitates bioactivity and osteoconductivity. Bioact. Mater. 6 (2), 490–502.
Shuai, C., Peng, B., Feng, P., Yu, L., Lai, R., Min, A., 2022. In situ synthesis of hydroxyapatite nanorods on graphene oxide nanosheets and their reinforcement in biopolymer scaffold. J. Adv. Res. 35, 13–24.
Ślósarczyk, A., Paszkiewicz, Z., Paluszkiewicz, C., 2005. FTIR and XRD evaluation of carbonated hydroxyapatite powders synthesized by wet methods. J. Mol. Struct. 744-747, 657–661.
Surya, P., Nithin, A., Sundaramanickam, A., Sathish, M., 2021. Synthesis and characterization of nano-hydroxyapatite from Sardinella longiceps fish bone and its effects on human osteoblast bone cells. J. Mech. Behav. Biomed. Mater. 119, 104501.
Taggart, T., Kerry, R.M., Norman, P., Stockley, I., 2002. The use of vancomycin-impregnated cement beads in the management of infection of prosthetic joints. J. Bone Joint Surg. (Br.) 84 (1), 70–72.
Tang, Z., Tan, Y., Ni, Y., Wang, J., Zhu, X., Fan, Y., et al., 2017. Comparison of ectopic bone formation process induced by four calcium phosphate ceramics in mice. Mater. Sci. Eng. C Mater. Biol. Appl. 70 (Pt 2), 1000–1010.
Tantavisut, S., Leanpolchareanchai, J., Wongrakpanich, A., 2022. Influence of chitosan and chitosan oligosaccharide on dual antibiotic-loaded bone cement: in vitro evaluations. PLoS One 17 (11), e0276604.
van Vugt, T.A.G., Arts, J.J., Geurts, J.A.P., 2019. Antibiotic-Loaded Polymethylmethacrylate Beads and Spacers in Treatment of Orthopedic Infections and the Role of Biofilm Formation. Front. Microbiol. 10, 1626.
Wee, C.Y., Lim, J.T., Koo, J., Tjieh Lim, Q.R., Zhao, Y., Yang, Z., et al., 2022. Investigating the degradation behaviour and characteristic changes of phase pure hydroxyapatite (HAp) microsphere scaffolds under static and dynamic conditions. Mater. Technol. 1-13.
Zhao, C., Wu, H., Ni, J., Zhang, S., Zhang, X., 2017. Development of PLA/Mg composite for orthopedic implant: Tunable degradation and enhanced mineralization. Compos. Sci. Technol. 147, 8–15.
Zhao, D., Zhu, T., Li, J., Cui, L., Zhang, Z., Zhuang, X., et al., 2021. Poly(lactic-co-glycolic acid)-based composite bone-substitute materials. Bioact. Mater. 6 (2), 346–360.
Zhu, T., Jiang, M., Zhang, M., Cui, L., Yang, X., Wang, X., et al., 2022. Biofunctionalized composite scaffold to potentiate osteoconduction, angiogenesis, and favorable metabolic microenvironment for osteonecrosis therapy. Bioact. Mater. 9, 446–460.
Zusho, Y., Kobayashi, S., Osada, T., 2020. Mechanical behavior of hydroxyapatite-poly (lactic acid) hybrid porous scaffold. Adv. Compos. Mater. 29 (6), 587–602.